



AELAS: Automatic ELAStic property derivations via high-throughput first-principles computation[☆]

S.H. Zhang, R.F. Zhang^{*}

School of Materials Science and Engineering, Beihang University, Beijing 100191, PR China

Center for Integrated Computational Materials Engineering, International Research Institute for Multidisciplinary Science, Beihang University, Beijing 100191, PR China

ARTICLE INFO

Article history:

Received 6 April 2017

Received in revised form 9 June 2017

Accepted 11 July 2017

Available online 6 August 2017

Keywords:

Elastic properties

High-throughput computation

First-principles calculation

Two-dimensional materials

ABSTRACT

The elastic properties are fundamental and important for crystalline materials as they relate to other mechanical properties, various thermodynamic qualities as well as some critical physical properties. However, a complete set of experimentally determined elastic properties is only available for a small subset of known materials, and an automatic scheme for the derivations of elastic properties that is adapted to high-throughput computation is much demanding. In this paper, we present the AELAS code, an automated program for calculating second-order elastic constants of both two-dimensional and three-dimensional single crystal materials with any symmetry, which is designed mainly for high-throughput first-principles computation. Other derivations of general elastic properties such as Young's, bulk and shear moduli as well as Poisson's ratio of polycrystal materials, Pugh ratio, Cauchy pressure, elastic anisotropy and elastic stability criterion, are also implemented in this code. The implementation of the code has been critically validated by a lot of evaluations and tests on a broad class of materials including two-dimensional and three-dimensional materials, providing its efficiency and capability for high-throughput screening of specific materials with targeted mechanical properties.

Program summary

Program title: AELAS

Program Files doi: <http://dx.doi.org/10.17632/f8fwg4j9tw.1>

Licensing provisions: BSD 3-Clause

Programming language: Fortran

Nature of problem: To automate the calculations of second-order elastic constants and the derivations of other elastic properties for two-dimensional and three-dimensional materials with any symmetry via high-throughput first-principles computation.

Solution method: The space-group number is firstly determined by the SPGLIB code [1] and the structure is then redefined to unit cell with IEEE-format [2]. Secondly, based on the determined space group number, a set of distortion modes is automatically specified and the distorted structure files are generated. Afterwards, the total energy for each distorted structure is calculated by the first-principles codes, e.g. VASP [3]. Finally, the second-order elastic constants are determined from the quadratic coefficients of the polynomial fitting of the energies vs strain relationships and other elastic properties are accordingly derived.

References

[1] <http://atztoigo.github.io/spglib/>.

[2] A. Meitzler, H.F. Tiersten, A.W. Warner, D. Berlincourt, G.A. Couquin, F.S. Welsh III, IEEE standard on piezoelectricity, Society, 1988.

[3] G. Kresse, J. Furthmüller, Phys. Rev. B 54 (1996) 11169.

© 2017 Elsevier B.V. All rights reserved.

1. Introduction

Material discovery based on high-throughput (HT) computation has become an emerging research field in the past decade because it promises to avoid time-consuming try and error experiments and to solve the issues related to progressive complexity of numerous materials [1]. HT approach is recognized as one core task

[☆] This paper and its associated computer program are available via the Computer Physics Communication homepage on ScienceDirect (<http://www.sciencedirect.com/science/journal/00104655>).

^{*} Corresponding author at: School of Materials Science and Engineering, Beihang University, Beijing 100191, PR China.

E-mail address: zrf@buaa.edu.cn (R.F. Zhang).

in “Materials Genome Initiative” strategic plan to generate a large database of material properties and dig out new knowledge by an automatic flow strategy from ideas to results [2]. Clearly, the progress of HT approach benefits mostly from the rapid development of modern computational technique and advanced parallel computing architecture that was unavailable before. A popular application of HT approach is known as the thermodynamic stability analysis, where, for a given combination of chemical elements, stable structures at low temperatures are identified, and meanwhile the generated large databases provide a platform for the exploration of new materials with targeted properties. Some representative databases generated by HT first-principles computation so far include the Materials Projects (MP) [3], the Automatic Flow for Materials Discovery (AFLOW) [4], the Open Quantum Materials Database (OQMD) [5], the Quantum Materials Informatics Project (QMIP) [6], and the Computational Materials Repository (CMR) [7]. Despite these databases provide the well suited codes with the implementation of high efficient HT computation, these codes however focus mostly on the structure stability and functional properties of materials. Except for the well-known MP code [8–11], few are designed for an automatic HT scheme to derive the mechanical properties, such as elastic constants, elastic anisotropy, mechanical stability, Poisson’s ratio, mechanical strength, stacking fault energy and Peierls–Nabarro stress. These parameters are critical in designing the advanced structural materials with desired mechanical properties, such as ultraincompressible materials, hard and superhard materials [12,13], metallic composites with high-strength and high-ductility, and superalloys [14].

Among various mechanical properties, the elastic property of a crystalline solid is a fundamental quality that describes a reversible response to external forces within elastic limit, playing an important role in designing structural materials. For instance, the elastic anisotropy of a crystal can be correlated to the thermodynamic properties, such as thermal expansion, melting point and Debye temperature [15], while the Pugh ratio (the ratio of the bulk to shear modulus G/K) [16] and Cauchy pressure $P_C = (c_{12} - c_{44})$ [17] are known as basic parameters to estimate the brittleness or ductility of a material. In Peierls–Nabarro dislocation model, the elastic energy factors K_e and K_s are scaled by the shear modulus G and the Poisson’s ratio ν of a crystalline material [18]. In addition, the thermodynamically stabilized crystal structure must also follow the criterion of mechanical stability which can be evaluated by the anisotropic elastic constants [19]. Moreover, the elastic properties are key parameters that are relevant to the interatomic forces, phonon dispersion, structural phase transformation, as well as the cohesion of solids. Nevertheless, a complete set of experimentally determined elastic constants is only available for a small subset of known materials so far [20]. A great challenge faced in experiments is to get the elastic properties of a large number of metastable phases that may be stabilized at high temperature and high pressure, or in nanoscale, because of the technical difficulty or uncertainty. In this regard, first-principles calculation within framework of density functional theory (DFT) provides an alternative solution to derive the elastic properties within a required precise by applying a series of strain patterns on a crystal at equilibrium. And meanwhile some open source programs have been developed recently for this purpose including Pymatgen [21], ElaStic [22], besides of the implementation of the same functionality into the commercial software like CASTEP [23], VASP [24] and CRYSTAL [25].

Among these open-source codes, Pymatgen has recently released its HT solution to calculate elastic properties of massive inorganic crystalline compounds in a consistent manner [8–11], but its deficiency may intrinsically limit its applications and other alternative ones are much demanded to provide necessary supplement. For instance, the stress–strain method adopted in the

code requires high precise first-principles calculation of stress. Furthermore, although the elastic constants of two-dimensional (2D) materials, a broad branch of new nanomaterials, can be derived by solving 2D materials as specific three-dimensional (3D) materials in Pymatgen, a separate code designed for the calculation of the elastic properties of 2D materials is also necessary for the following reasons: firstly, in comparison to 3D materials, a smaller set of distortion modes is required for 2D materials in the derivation of elastic constants; secondly, the derived elastic moduli based on a 3D model cannot be directly used for those of 2D materials. To best of our knowledge, the HT approach for the elastic constant calculation of 2D materials has also not been implemented in the other open-source codes so far. Therefore, we here present a fully automated program named AELAS that is developed for the HT implementation of elastic constant calculation and other derived elastic properties based on the energy-strain method. In AELAS code, both 3D materials and 2D materials are supported with special consideration of several abnormal cases in dealing with unstable phases. A complete set of elastic properties is automatically derived, including the elastic stiffness tensor, compliance tensor, average elastic modulus with Voigt–Reuss–Hill approximation for polycrystals, Pugh ratio, Cauchy pressure, elastic anisotropy and elastic stability criterion. Furthermore, the automatic feature of AELAS code in deriving elastic properties is well adapted to HT first-principles computation, providing not only an alternative for HT solution of elastic properties but also a supplement to the deficiency of other previous codes.

In this article, we shall first give an overview in Section 2 on the theoretical method to calculate the elastic constants of a single crystal and the derivation of other elastic properties. Secondly, the workflow and automated scheme of the AELAS code is presented in Section 3. Afterwards, the details of first-principles calculation are presented in Section 4 and the implementation and validity of the AELAS code has been comprehensively tested in Section 5 by a lot of evaluations and comparisons on a broad class of materials including both typical 2D and 3D materials with different types of chemical bonding (*i.e.* metallic, covalent and ionic). In the last Section 6, a brief summary is given with a few remarks on the further development of AELAS code.

2. Methodology

2.1. Elasticity theory

Within the linear region, the response of solids to external loading are described using the generalized Hooke’s law and the stress $\sigma = (\sigma_1, \sigma_2, \sigma_3, \sigma_4, \sigma_5, \sigma_6)$ is related with the strain $\varepsilon = (\varepsilon_1, \varepsilon_2, \varepsilon_3, \varepsilon_4, \varepsilon_5, \varepsilon_6)$ in the normal form as:

$$\sigma_i = \sum_{j=1}^6 c_{ij} \varepsilon_j \quad (1)$$

where the coefficients c_{ij} are the elastic stiffness constants of the crystal and $\varepsilon_1 = \varepsilon_{xx}$, $\varepsilon_2 = \varepsilon_{yy}$, $\varepsilon_3 = \varepsilon_{zz}$, $\varepsilon_4 = \varepsilon_{yz} + \varepsilon_{zy}$, $\varepsilon_5 = \varepsilon_{xz} + \varepsilon_{zx}$, $\varepsilon_6 = \varepsilon_{yx} + \varepsilon_{xy}$ are in Voigt notation [26] by simplifying a pair of Cartesian indices into a single integer $1 \leq i \leq 6$, *i.e.* $xx \rightarrow 1$, $yy \rightarrow 2$, $zz \rightarrow 3$, $yz \rightarrow 4$, $xz \rightarrow 5$, $xy \rightarrow 6$. Thus a 3×3 symmetric strain or stress matrix reduces to a vector with 6 independent components, and the elastic stiffness tensor is expressed by a 6×6 matrix. Eq. (1) is changed to the form

$$\varepsilon_i = \sum_{j=1}^6 s_{ij} \sigma_j \quad (2)$$

where s_{ij} are the elements of elastic compliance tensor that satisfies $[s_{ij}] = [c_{ij}]^{-1}$.

The internal energy of a crystal under strain ε can be represented by Taylor expansion in power of the strain tensor in the following equation:

$$E(V, \{\varepsilon_i\}) = E(V_0, 0) + V_0 \sum_i \sigma_i \varepsilon_i + \frac{V_0}{2} \sum_{i,j=1}^6 c_{ij} \varepsilon_i \varepsilon_j + \dots, \quad (3)$$

where $E(V_0, 0)$ and V_0 are the energy and volume of the reference structure (usually the equilibrium one), respectively.

In general, there are two methods for the first-principles calculation of elastic constants: energy-strain method and stress-strain method. The energy-strain method corresponds that the elastic stiffness tensor is derived from the second-order derivative of the total energies with respect to strain (i.e. Eq. (3)), while the stress-strain methodology is based on the first-order derivative of the stresses (i.e. Eq. (1)). The stress-strain method requires much smaller set of distortions than the energy-strain method, since there are six stress components that can be obtained for each DFT calculation whereas only one energy for each fitting [27]. Nevertheless, a much higher computational precise is required for stress-strain method to achieve the same accuracy as energy-strain method [22], which makes the former method apply mainly for the determination of stability of a structure within minor distortion. To reduce the stress sensitivity, the energy-strain method is therefore more favorable and used in AELAS code. In this method, one first chooses a set of distortion modes, e.g. $\varepsilon_I = (0, 0, 0, \delta, \delta, \delta)$, $\varepsilon_{II} = (\delta, \delta, 0, 0, 0, 0)$ and $\varepsilon_{III} = (\delta, \delta, \delta, 0, 0, 0)$ for cubic system, and then the strain energies are calculated for each distorted structure. After that, the quadratic coefficients are determined by fitting the energy-distortion δ relationship, and finally the second order elastic constants c_{ij} are determined.

2.2. Polycrystalline bulk and shear moduli

In a polycrystalline material, the crystallites are randomly oriented, and such materials can be considered to be quasi-isotropic or isotropic in a statistical sense. The elastic response of an isotropic system is generally described by the bulk modulus K and the shear modulus G , which may be obtained by averaging the single-crystal elastic constants [28]. The averaging methods most widely used are the Voigt [26] bound, Reuss [29] bound, Hashin-Shtrikman [30] bound and Hill [31] average. Voigt's procedure assumes that the strain is uniform throughout an aggregate, while the Reuss' one takes the stress to be uniform [31]. In Voigt's approximation, the equation takes the following form:

$$\begin{cases} 9K_V = (c_{11} + c_{22} + c_{33}) + 2(c_{12} + c_{23} + c_{31}) \\ 15G_V = (c_{11} + c_{22} + c_{33}) - (c_{12} + c_{23} + c_{31}) \\ \quad + 4(c_{44} + c_{55} + c_{66}), \end{cases} \quad (4)$$

while the Reuss bounds is that

$$\begin{cases} 1/K_R = (s_{11} + s_{22} + s_{33}) + 2(s_{12} + s_{23} + s_{31}) \\ 15/G_R = 4(s_{11} + s_{22} + s_{33}) - 4(s_{12} + s_{23} + s_{31}) \\ \quad + 3(s_{44} + s_{55} + s_{66}). \end{cases} \quad (5)$$

The Young's modulus E , and Poisson's ratio ν for an isotropic material are given by $E = \frac{9KG}{3K+G}$ and $\nu = \frac{3K-2G}{2(3K+G)}$, respectively.

Hill [31] has demonstrated that the Voigt and Reuss bounds are rigorous upper and lower bounds, respectively. The arithmetic mean of the Voigt and Reuss bounds, i.e. $K_{VRH} = 1/2(K_V + K_R)$ and $G_{VRH} = 1/2(G_V + G_R)$, termed the Voigt–Reuss–Hill (VRH) average is found as better approximation to the actual elastic behavior of a polycrystal material [31]. In weakly anisotropic materials, of course, all these averages lead to similar results for elastic moduli. Alternatively, one would prefer to use the geometric or harmonic means instead of the arithmetic average too.

2.3. Pugh ratio and Cauchy pressure

A well-established justification of whether a crystalline solid is ductile or brittle is if dislocation embryos can be more easily nucleated from a sharp crack tip prior to its propagation by cleavage [32,33]. The bifurcation in mechanical behavior can be represented by the ratio of the shear modulus to the bulk modulus, i.e. Pugh ratio G/K , by simply considering K as the resistance to fracture and G as the resistance to plastic deformation [16]. The critical value of G/K ratio to separate ductile and brittle materials is around 0.57. That means if $G/K < 0.57$ the material is more ductile, otherwise the material behaves in a brittle manner [16]. The higher G/K indicates the more brittleness of the material.

Cauchy pressure $P_C = (c_{12} - c_{44})$ is another quantity to describe the brittleness or ductility of a material by counting for the angular character of atomic bonding in the metals and compounds [17]. For covalent materials with brittle atomic bonds, the Cauchy pressure is negative ($c_{12} < c_{44}$), because in such case material resistance to shear strain (c_{44}) is much larger than that to volume change (c_{12}) [34]. In case of metallic-like bonding with delocalized electrons however, the Cauchy pressure should be positive ($c_{12} > c_{44}$) [17,34].

2.4. Elastic anisotropy

To quantify the anisotropy of cubic crystals, Zener [35] introduced $A = 2c_{44}/(c_{11} - c_{12})$, where c_{11} , c_{12} , and c_{44} are the three independent components of elastic stiffness constants. More recently, Chung and Buessem [36] proposed another empirical factor to measure elastic anisotropy of cubic crystals by a single-value as [36,37],

$$A^C = \frac{G_V - G_R}{G_V + G_R} = \frac{3(A - 1)^2}{3(A - 1)^2 + 25A}, \quad (6)$$

where G_V and G_R are the shear modulus with the Voigt and Reuss approximation, respectively, and A is the Zener anisotropy coefficient. Note that A^C is generally different if A^{-1} is used instead of A [37]. The two definitions of elastic anisotropy are helpful as long as one considers cubic crystals that exhibit an isotropic bulk resistance. For all other crystal types, the bulk response is in general anisotropic and one must account for such contributions in order to quantify the extent of anisotropy accurately. For this purpose, Ranganathan et al. [37] introduced a new universal anisotropy index that overcomes the above limitations:

$$A^U = 5 \frac{G_V}{G_R} + \frac{K_V}{K_R} - 6, \quad (7)$$

where K_V , K_R , G_V and G_R are the bulk and shear moduli with the Voigt and Reuss estimates, respectively. In the special case of cubic crystals, the relation between A^U and A takes the following form: $A^U = \frac{6}{5}(A^{1/2} - A^{-1/2})^2$ [37]. For an isotropic crystal, A^U is identically zero, and the departure of A^U from zero defines the extent of elastic anisotropy with considering both the shear and bulk contributions unlike all other existing anisotropy measures [37]. Thus, A^U represents a universal measure to quantify the single crystal elastic anisotropy [37].

2.5. Criterion of elastic stability

For a crystalline structure, the elastic stability criterion is defined as the elastic energy given by the quadratic form of Eq. (3). It is always positive [19] for a stable structure in the harmonic approximation [38]. As first noted by Born [39], it is mathematically equivalent to the following necessary and sufficient stability conditions: (i) The second-order elastic stiffness tensor matrix \mathbf{C} is definitely positive, (ii) all eigenvalues of \mathbf{C} are positive, (iii) all the

Table 1
Properties derived from the elastic constant matrix in AELAS code for 3D materials.

Property	Unit	Description	Equation	Ref.
Elastic tensor, $[c_{ij}]$	GPa	Tensor, describing elastic behavior (IEEE-format)	See main text	
Compliance tensor, $[s_{ij}]$	GPa ⁻¹	Tensor, describing elastic behavior	$[s_{ij}] = [c_{ij}]^{-1}$	
Bulk modulus Voigt average, K_V	GPa	Upper bound on K for polycrystalline material	$9K_V = (c_{11} + c_{22} + c_{33}) + 2(c_{12} + c_{23} + c_{13})$	[31]
Bulk modulus Reuss average, K_R	GPa	Lower bound on K for polycrystalline material	$1/K_R = (s_{11} + s_{22} + s_{33}) + 2(s_{12} + s_{23} + s_{13})$	[31]
Shear modulus Voigt average, G_V	GPa	Upper bound on G for polycrystalline material	$15G_V = (c_{11} + c_{22} + c_{33}) - (c_{12} + c_{23} + c_{13}) + 3(c_{44} + c_{55} + c_{66})$	[31]
Shear modulus Reuss average, G_R	GPa	Lower bound on G for polycrystalline material	$15/G_R = 4(s_{11} + s_{22} + s_{33}) - 4(s_{12} + s_{23} + s_{13}) + 3(s_{44} + s_{55} + s_{66})$	[31]
Bulk modulus Hill average, K_{VRH}	GPa	Average of K_V and K_R	$K_{VRH} = (K_V + K_R)/2$	[31]
Shear modulus Hill average, G_{VRH}	GPa	Average of G_V and G_R	$G_{VRH} = (G_V + G_R)/2$	[31]
Young's modulus Hill average, E_{VRH}	GPa	E for polycrystalline material	$E_{VRH} = 9K_{VRH}G_{VRH}/(3K_{VRH} + G_{VRH})$	[31]
Isotropic Poisson's ratio, ν_{VRH}	–	Number, describing lateral response to loading	$\nu_{VRH} = (3K_{VRH} - 2G_{VRH})/(6K_{VRH} + 2G_{VRH})$	[31]
Pugh ratio	–	Ductility–brittleness transition	G_{VRH}/K_{VRH}	[16]
Cauchy pressure, P_C	GPa	Ductility–brittleness transition	$P_C = c_{12} - c_{44}$	[17]
Chung–Buessem anisotropy index, A^C	–	Description of elastic anisotropy	$A^C = (G_V - G_R)/(G_V + G_R)$	[36]
Universal elastic anisotropy index, A^U	–	Description of elastic anisotropy	$A^U = 5G_V/G_R + K_V/K_R - 6$	[37]
Elastic stability criterion	–	Necessary and sufficient elastic stability conditions for crystal systems	See main text	[19]

leading principal minors of \mathbf{C} are positive, and (iv) an arbitrary set of minors of \mathbf{C} are all positive. These are four possible formulations of the Born elastic stability conditions for a crystal, which are valid regardless of the crystal symmetry.

Recently, Mouhat et al. [19] proposed necessary and sufficient elastic stability conditions as regards the elastic stability for various crystal systems. These more detailed criterions [19] can be used to identify elastic tensor corresponding to materials that are mechanically stable but are near an elastic instability with a small tolerance [8]. Taken cubic crystal system as an example, it is required that $c_{11} - c_{12} > 0$, $c_{11} + 2c_{12} > 0$ and $c_{44} > 0$ and a small tolerance could be used that $c_{11} - \varepsilon c_{12} > 0$, where ε is a value slightly greater than one [8].

Under minor distortion, the elastic stability criterion considers the dependence of pressure. The elastic constant tensor \mathbf{C} should be replaced by an new elastic stiffness tensor \mathbf{B} [40], i.e. $\mathbf{B} = \mathbf{C} + \mathbf{A}$, where the tensor \mathbf{A} depends only on the applied stress. For instance, the cubic crystal under the hydrostatic compression pressure ($P > 0$) [41]: $c_{11} + 2c_{12} + P > 0$, $c_{11} - c_{12} - 2P > 0$, $c_{44} - P > 0$.

2.6. Elasticity of 2D materials

For 2D materials, the elastic constants can also be derived from the Hooke's law under plane-stress condition [42]

$$\begin{bmatrix} \sigma_1 \\ \sigma_2 \\ \sigma_3 \end{bmatrix} = \begin{bmatrix} c_{11} & c_{12} & c_{16} \\ & c_{22} & c_{26} \\ & & c_{66} \end{bmatrix} \cdot \begin{bmatrix} \varepsilon_1 \\ \varepsilon_2 \\ \varepsilon_3 \end{bmatrix}. \quad (8)$$

Similar to 3D materials, the elastic stiffness constants can be calculated using the formula,

$$c_{ij} = \frac{1}{A_0} \left(\frac{\partial^2 E}{\partial \varepsilon_i \partial \varepsilon_j} \right), \quad (9)$$

where A_0 is the area of simulation cell in the x – y plane. The relation between the Young's and shear moduli, Poisson's ratios and elastic stiffness constants for a 2D system can be derived by [43]

$$E_x = \frac{c_{11}c_{22} - c_{12}c_{21}}{c_{22}}, E_y = \frac{c_{11}c_{22} - c_{12}c_{21}}{c_{11}}, \quad (10)$$

$$\nu_{xy} = \frac{c_{21}}{c_{22}}, \nu_{yx} = \frac{c_{12}}{c_{11}}, G_{xy} = c_{66},$$

where $E_i = \sigma_i/\varepsilon_i$ is the Young's modulus along the axis of i , $\nu_{ij} = -d\varepsilon_j/d\varepsilon_i$ is the Poisson's ratio with tensile strain applied in the direction i and the response strain in the direction j , and G_{xy} is the shear modulus in the x – y plane [43]. Note that since no particular thickness is assumed for a single atomic layer or a few atomic layers of 2D materials, the unit for the elastic stiffness tensor as well as the elastic moduli are actually force per unit length (N/m) rather than force per area (N/m² or Pa). A method of effective thickness has been used in many literatures [44,45]. According to this method, the relationship between elastic stiffness constants c_{ij} (unit: Pa) and c_{ij} (unit: N/m) is that: $c_{ij}(\text{Pa}) = c_{ij}(\text{N/m})/d_0$, where d_0 is the effective thickness of the system [45].

3. Workflow and automated scheme

In this section, we describe the workflow and automated scheme of the AELAS code using energy-strain method to compute elastic constants and other derived elastic properties listed in Tables 1 and 2. A fully-automated procedure with minimum input parameters is adapted to HT computation strategy in order to meet the demands for the generation of a large database of elastic data for material design. Note that it is assumed that the crystal structure has been preliminarily optimized for both lattice parameters and atomic positions before the calculation of elastic constants. The workflow of AELAS code is schematically shown in Fig. 1 and more details are discussed below:

Specify 2D or 3D materials

The type of either 2D or 3D material is chosen for the calculation of the elastic properties. To be noticed that for 2D materials, it is necessary that the lattice vector normal to the atomic layer must be sufficient large in order to avoid its interaction to its periodic image.

Read the structure data

An input structure file containing information of lattice vectors and atomic coordinates must be provided. For this purpose, the AELAS code requires a standard POSCAR or CONTCAR file if one uses VASP to do the first-principles calculation.

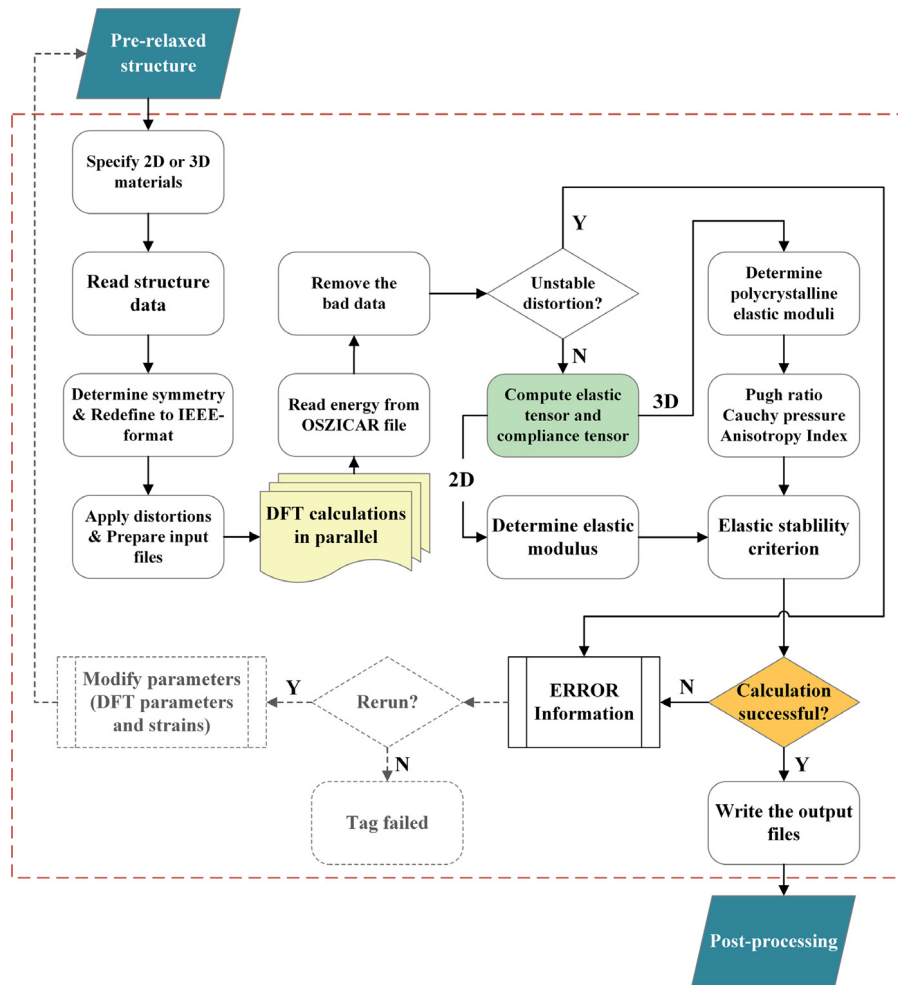


Fig. 1. Workflow of the algorithm used in the AELAS code (Figure 1 in Ref. [8] is referenced). The procedure of “Remove the bad data” corresponds to the filters: (i) the existence of bad data, while the “Unstable distortion?” includes the other three filters: (ii) it does not show quadratic relation, (iii) the structure is not at equilibrium, and (iv) the unstable distortion mode exists, as illustrated in Fig. 2.

Table 2

Properties derived from the elastic constant matrix in AELAS code for 2D materials.

Property	Unit	Description	Equation	Ref.
Elastic tensor, $[c_{ij}]$	N/m	Tensor, describing elastic behavior	See main text	
Compliance tensor, $[s_{ij}]$	$(\text{N/m})^{-1}$	Tensor, describing elastic behavior	$[s_{ij}] = [c_{ij}]^{-1}$	
Young's modulus in the x direction, E_x	N/m	–	$E_x = (c_{11}c_{22} - c_{12}c_{21})/c_{22}$	[43]
Young's modulus in the y direction, E_y	N/m	–	$E_y = (c_{11}c_{22} - c_{12}c_{21})/c_{11}$	[43]
Shear modulus, G_{xy}	N/m	Shear modulus on the x-y plane	$G_{xy} = c_{66}$	[43]
Poisson's ratio in the x direction, ν_{xy}	–	Number, describing lateral response to loading	$\nu_{xy} = c_{21}/c_{22}$	[43]
Poisson's ratio in the y direction, ν_{yx}	–	Number, describing lateral response to loading	$\nu_{yx} = c_{12}/c_{11}$	[43]
Elastic stability criterion	–	Necessary and sufficient elastic stability conditions for crystal systems	See main text	[19]

Determine the space group number and redefine to IEEE-format [46]

In order to determine how many independent elastic constants to be calculated, the space group number is firstly analyzed by the SPGLIB code [47]. A classification of the different crystal system with the corresponding number of independent elastic constants is given in Table 3 for 3D materials and Table 4 for 2D materials. In the meanwhile, the symmetry of the input structure is analyzed and accordingly the structure will be redefined to unit cell.

As the components of c_{ij} depend on the choice of coordinate system and lattice vectors, the IEEE-format [46] shown in Table 5 is adopted as standard representation for 3D materials. Table 6 gives the coordinate system and lattice vectors for 2D materials used in AELAS code, in which the c -axis is defined to be perpendicular to the atomic layers of 2D materials.

Distort the crystal and prepare input files

According to the determined space group number, a set of distortion modes will be specified and applied to the crystal structure with different values of strain around the equilibrium, and a series of distorted structure files are generated. Then, the input files of VASP are created for first-principles calculation to get the total energy of each distorted structure. Two default INCAR files can be chosen in AELAS code for structural relaxation and static calculation respectively. In order to calculate the elastic properties under high pressure, one may input the value of pressure when the INCAR file is created.

In AELAS code, there are two automatic methods to specify the KPOINTS file: the k -points per reciprocal atom (KPPRA) [48] and the smallest allowed spacing between k -points (KSPACING).

Table 3

Classification of crystal systems, point-group symbols and space-group number (S.G.N) are provided with the number of independent elastic constants for 3D materials. The material prototypes are shown in the last column.

Crystal system	Point group classes	S.G.N	Number of independent elastic constants	Material prototypes
Triclinic	$1, \bar{1}$	1–2	21	MnP ₄
Monoclinic	$m, 2, \frac{2}{m}$	3–15	13	M-Carbon, θ -Al ₂ O ₃ , CaMgSi ₂ O ₆
Orthorhombic	$222, mm2, \frac{2}{m} \frac{2}{m} \frac{2}{m}$	16–74	9	R-Carbon, PtSi, CdSb
Tetragonal I	$422, 4mm, 42m, \frac{4}{m} \frac{2}{m} \frac{2}{m}$	89–142	6	MgF ₂ , α -Pt ₂ Si, Anatase
Tetragonal II	$4, \bar{4}, \frac{4}{m}$	75–88	7	CaMoO ₄
Trigonal I	$32, 3m, \bar{3} \frac{2}{m}$	149–167	6	α -Al ₂ O ₃ , B ₆ O
Trigonal II	$3, \bar{3}$	143–148	7	CaMgC ₂ O ₆
Hexagonal	$622, 6mm, \bar{6}2m, \frac{6}{m} \frac{2}{m} \frac{2}{m}, 6, \bar{6}, \frac{6}{m}$	168–194	5	Mg, WC, BeO, ZnS
Cubic	$432, \bar{4}3m, \frac{4}{m} \frac{3}{m} \frac{2}{m}, 23, \frac{2}{m} \frac{3}{m} \frac{2}{m}$	195–230	3	Diamond, Cu, MgO

Table 4

Classification of crystal systems, 2D space groups and the independent elastic constants are provided with the number of independent elastic constants for 2D materials. The material prototypes are shown in the last column.

Crystal system	2D space groups	Independent elastic constants	Number of independent elastic constants	Material prototypes
Oblique	$p1, p2$	$c_{11}, c_{12}, c_{22}, c_{16}, c_{26}, c_{66}$	6	–
Rectangular	$pm, pg, p2mm, p2gg, p2mg, cm, c2mm,$	$c_{11}, c_{12}, c_{22}, c_{66}$	4	Borophene, B- and W-Graphane
Square	$p4, p4mm, p4gm,$	c_{11}, c_{12}, c_{66}	3	–
Hexagonal	$p3, p6, p3m, p3_1m, p6mm$	c_{11}, c_{12}	2	Graphene, MoS ₂ , Silicene, Ti ₂ C

Table 5

The IEEE-format [46] for 3D materials used in AELAS code.

Crystal system	Lattice constants		Axes		
			X	Y	Z
Triclinic	$c_0 < a_0 < b_0$	$\alpha \& \beta > 90^\circ$		$\perp(010)$	c
Monoclinic	$c_0 < a_0$	$\beta > 90^\circ, \alpha = \gamma = 90^\circ$	$\perp(100)$	b	c
Orthorhombic	$c_0 < a_0 < b_0$	$\alpha = \beta = \gamma = 90^\circ$	a	b	c
Tetragonal	$a_0 = b_0$	$\alpha = \beta = \gamma = 90^\circ$	(a_1)	(a_2)	c
Trigonal	$(a_0)_1 = (a_0)_2 = (a_0)_3$	$\alpha = \beta = 90^\circ, \gamma = 120^\circ$	(a_1)		c
Hexagonal	$(a_0)_1 = (a_0)_2 = (a_0)_3$	$\alpha = \beta = 90^\circ, \gamma = 120^\circ$	(a_1)		c
Cubic	$c_0 = a_0 = b_0$	$\alpha = \beta = \gamma = 90^\circ$	(a_1)	(a_2)	(a_3)

Table 6

The coordinate system and lattice vectors for 2D materials used in AELAS code. The c axis is perpendicular to the layer plane of 2D materials.

Crystal system	Lattice constants		Axes		
			X	Y	Z
Oblique	$b_0 < a_0$	$\gamma > 90^\circ, \alpha = \beta = 90^\circ$	a	$\perp(010)$	c
Rectangular	$b_0 < a_0$	$\alpha = \beta = \gamma = 90^\circ$	a	b	c
Square	$a_0 = b_0$	$\alpha = \beta = \gamma = 90^\circ$	(a_1)	(a_2)	c
Hexagonal	$(a_0)_1 = (a_0)_2 = (a_0)_3$	$\alpha = \beta = 90^\circ, \gamma = 120^\circ$	(a_1)		c

The KPPRA is a way to automatically set the k -point mesh while keeping the k -point density constant along the three axes despite of the variation of the unit cell. The number of mesh points along a given reciprocal lattice vector a_1 is set proportional to $|a_1 \cdot (a_2 \times a_3)|/|a_2 \times a_3|$, where a_2 and a_3 are the other two remaining reciprocal lattice vectors. The KSPACING is another automatic method that makes the mesh as uniform as possible. According to this method, the number of k -points in the direction of three reciprocal lattice vectors is determined by the equation: $|a_i|/KSPACING$.

Perform ab initio calculations and retrieve total energy from OSZICAR files

The total energies for a series of distorted structures generated at the previous step are calculated by the first-principles codes, e.g. VASP [24], and then the total energies of all distorted structures are retrieved from the generated OSZICAR files for processing in next step.

Avoid the unstable distortion

As illustrated in Fig. 2, the quadratic relation between total energy and strain δ is checked using various filters in order to detect abnormal case or possible fitting errors. The filters include: (i) the existence of bad data, (ii) it does not show quadratic relation, (iii) the structure is not at equilibrium, and (iv) the unstable distortion mode exists.

Solution to case (i) aims to avoid the fitting error induced by the bad data from first-principles calculation. As shown in Fig. 2a, the bad data has a big impact on the results of elastic constants (red line) and the AELAS code will remove the bad data before the fitting procedure (blue line). Solution to case (ii) shown in Fig. 2b, is used when there is no quadratic polynomial relationship between energies and δ , because of the calculation error or the lattice instability. Fig. 2c illustrates the case (iii), in which the initial structure is not at equilibrium. The case (iv) corresponds to the appearance of unstable distortion path of a structure, for instance,

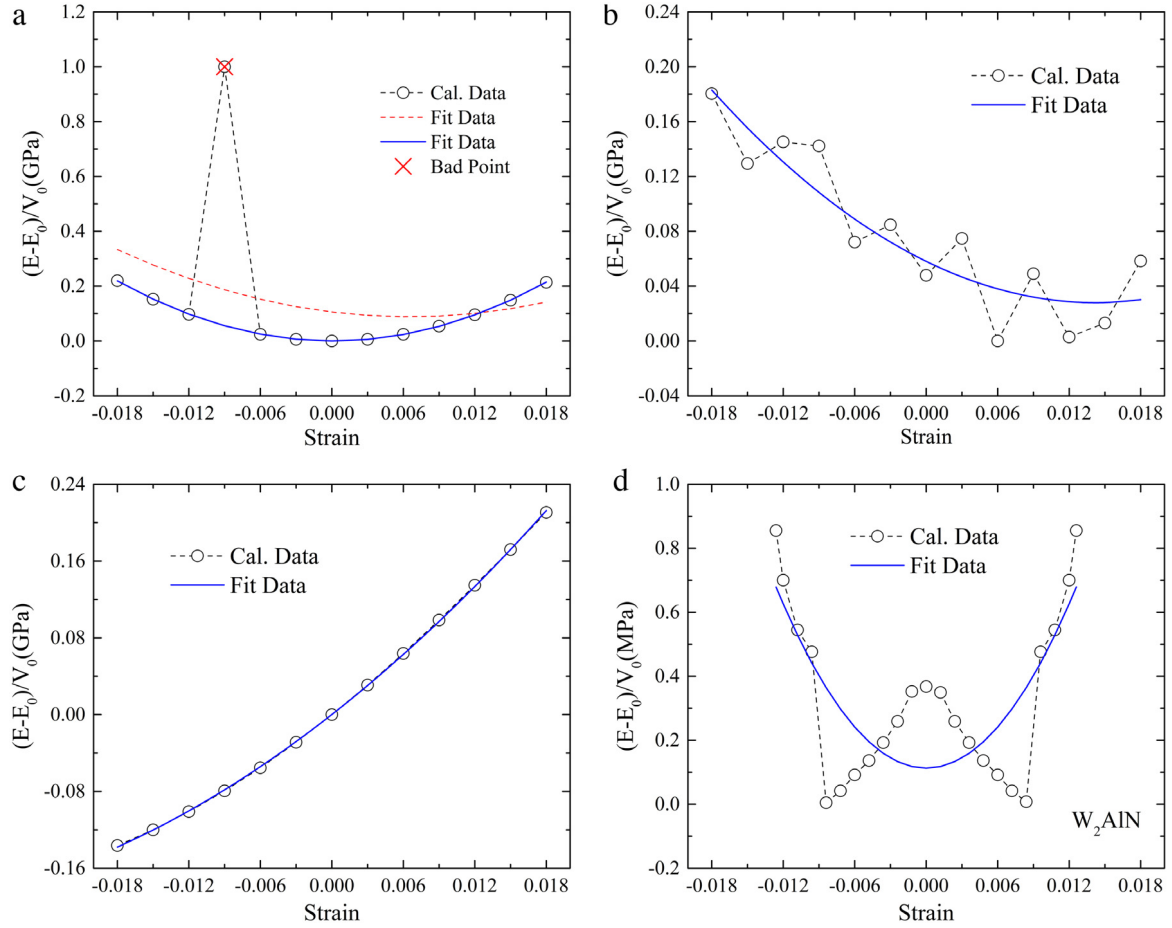


Fig. 2. The four filters implemented in AELAS code to resolve the calculation error, the physically unlikely behavior or lattice instabilities: (a) the existence of bad data, (b) it does not show quadratic relation, (c) the structure is not at equilibrium, and (d) the unstable distortion mode exists. (For interpretation of the references to color in this figure legend, the reader is referred to the web version of this article.)

the MAX phase [49] W_2AlN with distortion $\varepsilon = (0, 0, 0, \delta, \delta, 0)$ shown in Fig. 2d.

Calculate the elastic constants

A quadratic polynomial least square fitting procedure is applied to calculate the second derivative of the total energy vs δ , and then the quadratic coefficient is expressed as a linear combination of the elastic constants. This procedure is repeated for each inequivalent distortion mode, and finally a set of linear equations is solved to get the elastic constants.

Calculate the other elastic properties

The derived elastic properties are listed in Table 1 for 3D materials and Table 2 for 2D materials, including the relationship between single crystal elastic constants and those derived properties. In AELAS code, the polycrystalline Young's, bulk and shear moduli as well as Poisson's ratio are calculated by three averaging approaches widely used: Voigt [26], Reuss [29] and Hill [31] approximation. The Voigt approximation sets the upper bound of elastic modulus for polycrystalline materials, while Reuss approximation gives the lower bound of elastic modulus. The Hill approximation is the average of the Voigt and Reuss values. More details can be found in Section 2.2. The Pugh ratio [16] is calculated by means of the Hill value of shear and bulk moduli, i.e. G_{VRH}/K_{VRH} . The calculation of Chung-Buessem anisotropy index [36] and universal elastic anisotropy index [37] for a structure is also implemented in AELAS code. In addition, the generic necessary and sufficient criterion of elastic stability is used, which follows that all eigenvalues of \mathbf{C} are positive. Note that this elastic stability criterion is not applicable when the elastic constants are calculated under high pressure [40,41].

Filter of whether the calculation is successful

Another challenge in HT database generation is the implementation of automatic response to the calculation failure. For this purpose, an error or warning information system is necessary for AELAS code too. A filter will be used in AELAS code to justify whether the calculation is successful. If successful, the final results will be written to the output file, while if not, an error or warning information will be printed for further calculations.

4. Computational details

Our first-principles DFT calculations were performed using the Vienna *ab initio* simulation package (VASP) code [24] by the projector augmented wave (PAW) method [50] with the Perdew–Burke–Ernzerhof (PBE) version [51] of the Generalized Gradient Approximation (GGA) as the exchange–correlation functional for the non-carbon materials. While, for carbon materials calculated in this paper, i.e. Graphene, Diamond, R-carbon and M-carbon, the local density approximation (LDA) in the form of Ceperley–Alder [52,53] was used as the exchange–correlation functional. The energy convergence criterion of the electronic self-consistency was chosen as 10^{-6} eV/cell, while the force convergence criterion of ionic relaxation was used, with all forces acting on atoms being lower than 10^{-3} eV/Å. The Gaussian method [54] was used for electronic self-consistency calculation with a smearing width of 0.01 eV. In all calculations, an energy cutoff of 520 eV was applied. For non-metal 3D materials, the Monkhorst–Pack k -mesh [55] gamma-centered grids with 4000 k -points per reciprocal atom

Table 7

Elastic constants (c_{ij}) for Graphene, MoS₂, Silicene and Ti₂C with hexagonal structure and Borophenes, B- and M-graphane with rectangular structure are compared with the previous theoretical values [56–62]. The Young's (E_x and E_y) and shear (G_{xy}) moduli as well as Poisson's ratio (ν_{xy} and ν_{yx}) are also provided.

Crystal system	Material prototype	c_{11}	c_{12}	c_{22}	c_{66}	E_x	E_y	G_{xy}	ν_{xy}	ν_{yx}	Ref.
Hexagonal	Graphene	352.69	81.79			333.72	333.72		0.232	0.232	This work
		358.1	60.4								Cal. [56]
	MoS ₂	132.45	33.00			124.22	124.22		0.249	0.249	This work
		130	40								Cal. [57]
	Silicene	128.4	32.6			70.82	70.82		0.406	0.406	Cal. [58]
		84.76	34.37								This work
	Ti ₂ C	84.8	34.1								Cal. [59]
		137.92	34.46			129.31	129.31		0.250	0.250	This work
Rectangular	Borophenes	137	32								Cal. [60]
		165.57	−0.41	387.56	76.63	165.57	387.56		−0.001	−0.002	This work
	B-graphane	170	−7	398	94						Cal. [61]
		227.59	−1.91	259.83	93.11	227.58	259.81		−0.007	−0.008	This work
	W-graphane	225	−1.7	258	93						Cal. [62]
		119.22	14.88	279.02	81.25	118.42	277.16		0.053	0.125	This work
		121	14	280	81						Cal. [62]

(KPPRA) [48] were used. While for the metals, *i.e.* Cu and Mg, we employed a high KPPRA of 20000 to keep the same accuracy with the ionic and covalent materials. For 2D materials, well-converged results were obtained using a Gamma-centered k -mesh grid $21 \times 21 \times 1$.

In this paper, with 13 values chosen for the strain magnitude, a maximum strain of 1.8% was applied initially to distort the structures, which is small enough to remain well within the linear-elastic regime.

5. Evaluations and discussions

5.1. Hexagonal and rectangular system of 2D materials

For 2D materials, the hexagonal system has the highest symmetry with only two independent elastic constants, c_{11} and c_{12} , and the elastic stiffness matrix is

$$C_{hex} = \begin{vmatrix} c_{11} & c_{12} & 0 \\ & c_{11} & 0 \\ & & c_{66} \end{vmatrix}, \quad (11)$$

where, in the hexagonal case, $c_{66} = (c_{11} - c_{12})/2$. For rectangular system, the elastic stiffness matrix has the following form with four independent elastic constants:

$$C_{rect} = \begin{vmatrix} c_{11} & c_{12} & 0 \\ & c_{22} & 0 \\ & & c_{66} \end{vmatrix}. \quad (12)$$

Table 7 presents the calculated elastic constants (c_{ij}) for Graphene, MoS₂, Silicene and Ti₂C with hexagonal structure and Borophene, B- and W-graphane with rectangular structure together with the previous theoretical values [56–62]. The Young's (E_x and E_y) and shear (G_{xy}) moduli as well as Poisson's ratio (ν_{xy} and ν_{yx}) are also provided in Table 7 for comparison, and it is shown that all calculated values by AELAS code are in reasonable agreement with the previous theoretical values [56–62], confirming the validity of AELAS code for 2D materials.

5.2. Cubic system

For cubic system, we have chosen three representative materials, *i.e.* Diamond, Cu and MgO for evaluation of our AELAS code. Table 8 lists the calculated elastic constants (c_{ij}) for single-crystal Diamond, Cu and MgO together with the experimental data [63,64] and other theoretical values [8,65,66]. The isotropic bulk (K_{VRH}) and shear (G_{VRH}) moduli obtained using the Hill approximation and the

universal anisotropy index (A^U) are also provided in Table 8, and it is seen that all the theoretical values for the three materials show a good agreement with the experimental data [63,64] and previous theoretical values [8,65,66].

5.3. Hexagonal and trigonal system

The elastic constants for Mg, WC, BeO and ZnS with hexagonal structure together with the experimental data [67] and other theoretical values [68–70] are compared in Table 8. It is found that whether the material is metallic type (Mg), ionic type (BeO), or covalent type (WC), our calculated values are in excellent agreement with the experimental [67] and other theoretical values [68–70].

In case of trigonal system, there are either six or seven independent elastic constants, which can be distinguished according to the space group number (see Table 3). For the trigonal I system, there are six independent elastic constants. To demonstrate the capability of AELAS code to apply for this system, the α -Al₂O₃ and B₆O are chosen for comparison. As listed in Table 9, our calculated results agree well with the experimental [71] and other theoretical values [72,73]. To be noted that only five elastic constants for B₆O are provided in the previous literatures [73–75].

For trigonal II system, there is one more independent elastic constant, namely c_{15} . The CaMgC₂O₆ is chosen as an example for the justification of AELAS code for this class of crystal structure, and the comparison is given in Table 9. Our results shows a good agreement with previous theoretical values [22] too. It is interestingly found that the universal anisotropy index for CaMgC₂O₆ ($A^U = 1.516$) is much higher than those of α -Al₂O₃ ($A^U = 0.147$) and B₆O ($A^U = 0.194$), which indicates that CaMgC₂O₆ is more elastically anisotropic than α -Al₂O₃ and B₆O.

5.4. Tetragonal and orthorhombic system

The tetragonal I crystal system has six independent elastic constants, while in case of the tetragonal II system, an additional elastic constant, c_{16} need to be included. A comparison of elastic properties of several materials in tetragonal I and II structure (MgF₂, Pt₂Si and Anatase for tetragonal I, and CaMoO₄ for tetragonal II system) are provided in Table 9. Our calculated values by AELAS code show a reasonable agreement with experimental data [76] and previous theoretical values [22,77–79].

The elastic stiffness tensor matrix of orthorhombic system has nine independent elastic constants. Table 9 lists the calculated elastic constants of R-carbon, PtSi and CdSb with orthorhombic structure and compared with previous theoretical values [8,80].

Table 8

Elastic constants (c_{ij}) for Diamond, Cu and MgO with cubic structure and Mg, WC, BeO and ZnS with hexagonal structure are compared with the experimental data [63,64,67] and other theoretical values [8,65,66,68–70]. The isotropic bulk (K_{VRH}) and shear (G_{VRH}) moduli obtained using the Hill approximation and the universal anisotropy index (A^U) are also provided.

Crystal system	Material prototype	c_{11}	c_{12}	c_{44}	c_{12}	c_{13}	K_{VRH}	G_{VRH}	A^U	Ref.
Cubic	Diamond	1104.53	153.01	594.09			470.18	543.54	0.059	This work
		1107	149	594			468	545		Cal. [65]
	Cu	171.63	121.52	73.83			24.36	14.97	0.146	This work
		177	125	81						Exp. [63]
	MgO	277.23	91.45	143.68			153.38	120.63	0.232	This work
		273.41	90.54	141.38			151.50	118.71		Cal. [8]
		297.0	97.2	155.7						Exp. [64]
		291	91	139						Cal. [66]
Hexagonal	Mg	69.12	21.84	20.01	70.84	16.37	20.70	36.98		This work
		63.1	22.2	22.7	66.3	22.6				Cal. [70]
	WC	729.24	949.93	305.72	230.36	185.84	399.76	289.83	0.105	This work
		697.3	955.4	310.3	251.4	190.6				Cal. [69]
	BeO	430.44	465.24	137.87	117.72	83.44	210.29	154.76	0.071	This work
		460.6	491.6	147.7	126.5	88.48				Exp. [67]
	ZnS	439.1	463	142.1	105	72				Cal. [68]
		114.73	134.25	27.58	51.46	39.22	69.26	32.36	0.185	This work
		124.2	140.0	28.64	60.15	45.54				Exp. [67]

It is seen that an agreement is obtained for the three orthorhombic crystals, indicating the successful implementation of AELAS code for this class of crystal structure.

5.5. Monoclinic and triclinic system

Monoclinic crystal system has 13 independent elastic constants. For comparison, Table 10 presents the calculated elastic constants for M-carbon, $\text{CaMgSi}_2\text{O}_6$ and $\theta\text{-Al}_2\text{O}_3$ together with the experimental data [81,82] and other theoretical values [72,83], and an agreement is reached for each material.

In case of triclinic crystal system, there are 21 independent components of the elastic stiffness tensor that need to be determined. Because it demands much computationally expensive first-principles calculation, we chose only one representative material MnP_4 to demonstrate the capability of our AELAS code. A comparison with previous theoretical values [8] is provided in Table 11, and the agreement provides a validation of the implementation of AELAS code for triclinic crystal structure system.

5.6. Elastic properties under high pressure

Fig. 3 shows the elastic constants of MgO under high pressure 0–55 GPa together with the experimental data by Zha et al. [64] and other theoretical values by Karki et al. [66], as well as those of B_6O under 0–240 GPa together with other theoretical values by Lu et al. [75] and Zhang et al. [73]. As illustrated in Fig. 3, our calculated results agree mostly with previous theoretical values. However, in case of MgO, it is found that the calculated values deviate gradually from the experimental data with the increase of pressure, which is mostly due to the non-volume-reservation distortion modes used in AELAS code.

6. Summary and perspective

In summary, the implementation and validation of AELAS code, an automatic derivation of elastic property for a broad class of materials including 2D and 3D materials via HT first-principles computation, have been presented. The automation and high efficiency demonstrate its promise as an effective tool for high-throughput screening of specific materials with targeted mechanical properties.

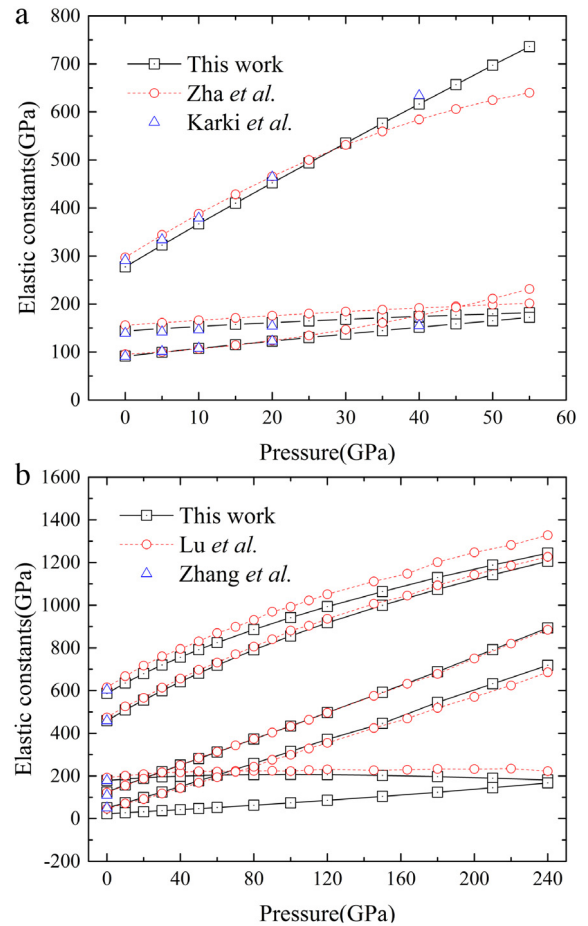


Fig. 3. The variation of elastic constants of (a) MgO under pressure ranging from 0 to 55 GPa together with the experimental data by Zha et al. [64], and other theoretical values by Karki et al. [66], as well as (b) B_6O under pressure ranging from 0 to 240 GPa together with other theoretical values by Lu et al. [75] and Zhang et al. [73].

We are currently advancing the AELAS code to support more first-principles codes and novel functionalities such as temperature-dependent elastic constants and volume reserved derivation of elastic constants for all crystal system.

Table 9

Elastic constants (c_{ij}) for α -Al₂O₃, B₆O and CaMgC₂O₆ with trigonal structure, MgF₂, Pt₂Si, Anatase and CaMoO₄ with tetragonal structure and R-carbon, PtSi and CdSb with orthorhombic structure are compared with the experimental data [71,76] and other theoretical values [8,22,72,73,77–80]. The isotropic bulk (K_{VRH}) and shear (G_{VRH}) moduli obtained using the Hill approximation as well as the universal anisotropy index (A^{U}) are also provided.

Crystal system	Material prototype	c_{11}	c_{22}	c_{33}	c_{44}	c_{55}	c_{66}	c_{12}	c_{13}	c_{23}	c_{14}	c_{15}	c_{16}	K_{VRH}	G_{VRH}	A^{U}	Ref.
Trigonal	α -Al ₂ O ₃	455.8		457.82	133.74			148.38	108.1		19.66			233.18	151.23	0.147	This work
		451.5		454.9	131.7			148.4	107.6		20.2						Cal. [72]
		497		501	147			163	116		22						Exp. [71]
	B ₆ O	586.83		459.06	178.38			124.67	50.63		22.72			228.45	207.96	0.194	This work
		603		459	179			109	50		–						Cal. [73]
	CaMgC ₂ O ₆	193.09		105.8	37.99			65.39	55.93		17.1	–13.48		89.83	43.54	1.516	This work
		194.3		108.5	38.8			66.5	56.8		17.5	–11.5					Cal. [22]
	MgF ₂	128.44		191.19	51.34		87.6	84.17	60.5					94.90	49.31	1.125	This work
		127.0		187.7	50.8		92.3	80.1	57.3								Cal. [22]
	α -Pt ₂ Si	299.65		280.86	60.57		163.19	208.68	147.85					208.41	74.81	1.064	This work
		324.8		281.2	71.0		172.2	215.3	182.5								Cal. [77]
		332.4		298.86	62.7		169.3	239.6	169.4								Cal. [78]
Tetragonal	Anatase	342.73		185.53	45.4		56.67	154.35	147.92					186.06	54.63	0.687	This work
		320		190	54		60	151	143								Cal. [79]
	CaMoO ₄	130.92		112.31	30.78		38.61	54.4	46.44				12.31	73.95	34.25	0.283	This work
		123.4		109.3	31.5		37.4	43.9	48.7				8.1				Cal. [22]
		144.7		126.5	36.9		45.1	66.4	46.6				13.4				Exp. [76]
	R-carbon	1030.68	1024.54	1160.14	508.39	397.21	458.21	190.39	49.8	104.37				433.74	461.02	0.069	This work
		1034.1	1025.5	1161	507.4	397.6	463	186.9	49.5	107.4				434.2	462.4		Cal. [80]
Orthorhombic	PtSi	260.61	277.17	244.73	90.04	52.75	92	117.3	130.34	144.54				173.92	70.93	0.300	This work
		263.31	279.29	247.80	86.10	49.31	89.46	116.40	128.53	144.76							Cal. [8]
	CdSb	68.98	63.03	57.05	22.5	20.6	12.95	27.09	30.13	25.05				17.96	39.11	0.219	This work
		68.55	63.64	56.98	22.28	18.59	12.75	26.80	30.13	24.72							Cal. [8]

Table 10

Elastic constants (c_{ij}) for M-carbon, $\text{CaMgSi}_2\text{O}_6$ and $\theta\text{-Al}_2\text{O}_3$ with monoclinic structure are compared with the experimental data [81,82] and other theoretical values [72,83]. The isotropic bulk (K_{VRH}) and shear (G_{VRH}) moduli obtained using the Hill approximation as well as the universal anisotropy index (A^{U}) are also provided.

Crystal system	Material prototype	c_{11}	c_{22}	c_{33}	c_{44}	c_{55}	c_{66}	c_{12}	c_{13}	c_{15}	c_{23}	c_{25}	c_{35}	c_{46}	K_{VRH}	G_{VRH}	A^{U}	Ref.
Monoclinic	M-carbon	981.28	1155.06	1099.6	546	474.31	397.99	59.36	185.75	67.18	104.05	−31.04	28.98	−10.49	471.23	435.70	0.111	This work
		926	1085	1046	522	453	394	43	147	67	80	−29	22	−6				Cal. [83]
	$\text{CaMgSi}_2\text{O}_6$	209.65	163.90	213.16	70.01	59.75	71.59	61.16	61.16	12.79	50.06	9.68	43.70	8.99	100.92	64.44	0.489	This work
		228.1	181.1	245.4	78.9	68.2	78.1	78.8	70.2	7.9	61.1	5.9	39.7	6.4				Exp. [81]
		229.0	179.0	242.5	78.9	68.1	78.2	78.0	69.8	9.9	69.8	6.1	40.9	6.6	114.6	72.7		Exp. [82]
	$\theta\text{-Al}_2\text{O}_3$	252.93	390.16	387.32	66.7	119.29	128.06	116.51	152.05	−0.78	59.68	0.89	21.5	6.11	186.15	102.54	0.756	This work
		269.1	389.3	404.2	74.2	102.2	126.0	113.2	132.2	−25.1	64.2	13.7	13.9	19.8				Cal. [72]

Table 11
Elastic constants (c_{ij}) for MnP_4 with triclinic structure are compared with the previous theoretical values [8]. The isotropic bulk (K_{VRH}) and shear (G_{VRH}) moduli obtained using the Hill approximation as well as the universal anisotropy index (A^{U}) are also provided.

Crystal system	Material prototype	c_{11}	c_{22}	c_{33}	c_{44}	c_{55}	c_{66}	c_{12}	c_{13}	c_{14}	c_{15}	c_{16}	c_{23}	c_{24}
Triclinic	MnP_4	293.49	293.73	317.66	101.78	163.82	88.84	44.05	89.78	16.5	1.28	−1.52	40.58	−17.47
		291.48	292.71	316.39	100.34	161.42	87.69	42.13	89.07	16.1	0.71	−1.31	39.31	−17.5
		c_{25}	c_{26}	c_{34}	c_{35}	c_{36}	c_{45}	c_{46}	c_{56}	K_{VRH}	G_{VRH}	A^{U}		Ref.
		−2.12	−3.27	−15.57	1.72	−2.25	−0.96	1.49	9.51	138.57	115.73	0.355		This work
		−2.06	−3.51	−15.35	2.06	−2.61	−0.83	1.64	9.26	137.20	114.76			Cal. [8]

Acknowledgments

This work is supported by the Fundamental Research Funds for the Central Universities, National Natural Science Foundation of China (NSFC) with Nos. 51471018 and 51672015, National Key Research and Development Program of China (Nos. 2016YFC1102500 and 2017YFB0702100) and National Thousand Young Talents Program of China.

Appendix A. Four filters used in AELAS code

(a) The existence of bad data

If the value of $(E - E_0)/V_0$ is outside the range of $0 \sim 1$, the data is considered as a bad data in AELAS code because the first-principles calculation may get non-convergent results. In this formula, E_0 and V_0 are the energy and volume of the reference structure (usually the equilibrium one), respectively, and E is the energy of the distorted structure under strain δ . In appearance of this case, the bad data will be removed, and the elastic constants are calculated based on the remaining data, as illustrates in Fig. 2a. Usually, by removing the bad data, the final results of elastic properties are not affected by the bad data.

(b) It does not show quadratic relation

In AELAS, the explained sum of squares is calculated when the quadratic polynomial fitting the relationship between $(E - E_0)/V_0$ and δ . If the value of the explained sum of squares is larger than 0.1, it is regarded that no quadratic relation exists between the energy and strain (see Fig. 2b), and therefore this case is considered as an error and no results are printed out.

(c) The structure is not at equilibrium

If the extreme point $-b/2a$ of the quadratic fitting polynomial $(E - E_0)/V_0 = a\delta^2 + b\delta + c$ is beyond the range $-0.004 \sim 0.004$, (see Fig. 2c), the structure is supposed to be not at equilibrium, and an error message is printed out.

(d) The unstable distortion mode exists

If the sign of the slope, defined as $(E_i - E_{i-1})/(\delta_i - \delta_{i-1})$, changes greater than 2 (for the normal case, i.e. with quadratic relation, the sign changes once), it is considered that the unstable distortion mode exists (see Fig. 2d). In this formula, δ_{i-1} , δ_i , E_{i-1} and E_i are the $(i-1)$ th and i th value of strain and the corresponding energy, respectively. Then, an error message is printed out, indicating that no reliable elastic properties are obtained.

Appendix B. Elastic stiffness tensor matrix for each crystal system

For cubic system, there are three independent elastic constants expressed in an elastic stiffness tensor matrix:

$$C_{cubic} = \begin{pmatrix} c_{11} & c_{12} & c_{12} & 0 & 0 & 0 \\ & c_{11} & c_{12} & 0 & 0 & 0 \\ & & c_{11} & 0 & 0 & 0 \\ & & & c_{44} & 0 & 0 \\ & & & & c_{44} & 0 \\ & & & & & c_{44} \end{pmatrix}. \quad (13)$$

For hexagonal system, there are five independent elastic constants with addition of the relation $c_{66} = (c_{11} - c_{12})/2$ and the elastic stiffness tensor matrix is expressed by

$$C_{hexa} = \begin{pmatrix} c_{11} & c_{12} & c_{13} & 0 & 0 & 0 \\ & c_{11} & c_{13} & 0 & 0 & 0 \\ & & c_{33} & 0 & 0 & 0 \\ & & & c_{44} & 0 & 0 \\ & & & & c_{44} & 0 \\ & & & & & c_{66} \end{pmatrix}. \quad (14)$$

In case of trigonal system, there are either six or seven independent elastic constants, which can be distinguished according to the

space group number (see Table 3). For the trigonal I system, the six independent elastic stiffness tensor is expressed in matrix form as:

$$C_{trig I} = \begin{pmatrix} c_{11} & c_{12} & c_{13} & c_{14} & 0 & 0 \\ & c_{11} & c_{13} & -c_{14} & 0 & 0 \\ & & c_{33} & 0 & 0 & 0 \\ & & & c_{44} & 0 & 0 \\ & & & & c_{44} & c_{14} \\ & & & & & c_{66} \end{pmatrix}, \quad (15)$$

where, $c_{66} = (c_{11} - c_{12})/2$ holds for hexagonal case.

For trigonal II system, there is one more independent elastic constant, namely c_{15} and the elastic stiffness tensor matrix is changed to

$$C_{trig II} = \begin{pmatrix} c_{11} & c_{12} & c_{13} & c_{14} & c_{15} & 0 \\ & c_{11} & c_{13} & -c_{14} & -c_{15} & 0 \\ & & c_{33} & 0 & 0 & 0 \\ & & & c_{44} & 0 & -c_{15} \\ & & & & c_{44} & c_{14} \\ & & & & & c_{66} \end{pmatrix}. \quad (16)$$

The tetragonal I crystal system has six independent elastic constants and the elastic stiffness tensor matrix is expressed by

$$C_{tetra I} = \begin{pmatrix} c_{11} & c_{12} & c_{13} & 0 & 0 & 0 \\ & c_{11} & c_{13} & 0 & 0 & 0 \\ & & c_{33} & 0 & 0 & 0 \\ & & & c_{44} & 0 & 0 \\ & & & & c_{44} & 0 \\ & & & & & c_{66} \end{pmatrix}. \quad (17)$$

In case of the tetragonal II system, an additional elastic constant, c_{16} need to be included and the elastic stiffness tensor matrix is changed to

$$C_{tetra II} = \begin{pmatrix} c_{11} & c_{12} & c_{13} & 0 & 0 & c_{16} \\ & c_{11} & c_{13} & 0 & 0 & -c_{16} \\ & & c_{33} & 0 & 0 & 0 \\ & & & c_{44} & 0 & 0 \\ & & & & c_{44} & 0 \\ & & & & & c_{66} \end{pmatrix}. \quad (18)$$

The elastic stiffness tensor matrix of orthorhombic system with nine independent elastic constants has the following form:

$$C_{ortho} = \begin{pmatrix} c_{11} & c_{12} & c_{13} & 0 & 0 & 0 \\ & c_{22} & c_{23} & 0 & 0 & 0 \\ & & c_{33} & 0 & 0 & 0 \\ & & & c_{44} & 0 & 0 \\ & & & & c_{55} & 0 \\ & & & & & c_{66} \end{pmatrix}. \quad (19)$$

Monoclinic crystal system has 13 independent elastic constants that are expressed in matrix form as:

$$C_{mono} = \begin{pmatrix} c_{11} & c_{12} & c_{13} & 0 & c_{15} & 0 \\ & c_{22} & c_{23} & 0 & c_{25} & 0 \\ & & c_{33} & 0 & c_{35} & 0 \\ & & & c_{44} & 0 & c_{46} \\ & & & & c_{55} & 0 \\ & & & & & c_{66} \end{pmatrix}. \quad (20)$$

In case of triclinic crystal system, there are 21 independent components of the elastic stiffness tensor that need to be determined:

$$C_{tric} = \begin{pmatrix} c_{11} & c_{12} & c_{13} & c_{14} & c_{15} & c_{16} \\ & c_{22} & c_{23} & c_{24} & c_{25} & c_{26} \\ & & c_{33} & c_{34} & c_{35} & c_{36} \\ & & & c_{44} & c_{45} & c_{46} \\ & & & & c_{55} & c_{56} \\ & & & & & c_{66} \end{pmatrix}. \quad (21)$$

Appendix C. The degree of automation in AELAS code

Two bash shell codes (*i.e.* *example/example3d.sh* for 3D materials and *example/example2d.sh* for 2D materials) has been provided for the pre-processing, first-principles calculations and post-processing, and no human intervention is required until the final results (including elastic constants and various elastic properties derived from elastic constants) are obtained. A bash shell code (*example/BatchCal.sh*) is also provided to calculate the elastic constants in batches.

References

- [1] K.S. Thygesen, K.W. Jacobsen, *Science* 354 (2016) 180–181.
- [2] S. Curtarolo, G.L.W. Hart, M.B. Nardelli, N. Mingo, S. Sanvito, O. Levy, *Nature Mater.* 12 (2013) 191–201.
- [3] A. Jain, S.P. Ong, G. Hautier, W. Chen, W.D. Richards, S. Dacek, S. Cholia, D. Gunter, D. Skinner, G. Ceder, *APL Mater.* 1 (2013) 011002.
- [4] S. Curtarolo, W. Setyawan, G.L. Hart, M. Jahnatek, R.V. Chepulska, R.H. Taylor, S.D. Wang, J.K. Xue, K.S. Yang, O. Levy, *Comput. Mater. Sci.* 58 (2012) 218–226.
- [5] J.E. Saal, S. Kirklin, M. Aykol, B. Meredig, C. Wolverton, *JOM* 65 (2013) 1501–1509.
- [6] <http://www.qmip.org/>.
- [7] D.D. Landis, J.S. Hummelshøj, S. Nestorov, J. Greeley, M. Dułak, T. Bligaard, J.K. Nørskov, K.W. Jacobsen, *Comput. Sci. Eng.* 14 (2012) 51–57.
- [8] M. De Jong, W. Chen, T. Angsten, A. Jain, R. Notestine, A. Gamst, M. Sluiter, C.K. Ande, S. Van Der Zwaag, J.J. Plata, *Sci. Dat.* 2 (2015).
- [9] M. de Jong, D.L. Olmsted, A. van de Walle, M. Asta, *Phys. Rev. B* 86 (2012) 224101.
- [10] M. de Jong, W. Chen, R. Notestine, K. Persson, G. Ceder, A. Jain, M. Asta, A. Gamst, *Sci. Rep.* 6 (2016).
- [11] M. De Jong, W. Chen, H. Geerlings, M. Asta, K.A. Persson, *Sci. Dat.* 2 (2015).
- [12] M.L. Cohen, *Solid State Commun.* 92 (1994) 45–52.
- [13] H.Y. Chung, M.B. Weinberger, J.M. Yang, S.H. Tolbert, R.B. Kaner, *Appl. Phys. Lett.* 92 (2008) 261904.
- [14] C. Nyshadham, C. Oses, J.E. Hansen, I. Takeuchi, S. Curtarolo, G.L. Hart, *Acta Mater.* 122 (2017) 438–447.
- [15] O.L. Anderson, *J. Phys. Chem. Solids* 24 (1963) 909–917.
- [16] S.F. Pugh, *London Edinburgh Dublin Philos. Maga. J. Sci.* 45 (1954) 823–843.
- [17] D.G. Pettifor, *Mater. Sci. Technol.* 8 (1992) 345–349.
- [18] V. Bulatov, W. Cai, *Computer Simulations of Dislocations*, Oxford University Press on Demand, 2006.
- [19] F. Mouhat, F.X. Coudert, *Phys. Rev. B* 90 (2014) 224104.
- [20] G. Simmons, H. Wang, *Single Crystal Elastic Constants and Calculated Aggregate Properties-A Handbook*, MIT Press, 1971.
- [21] S.P. Ong, W.D. Richards, A. Jain, G. Hautier, M. Kocher, S. Cholia, D. Gunter, V.L. Chevrier, K.A. Persson, G. Ceder, *Comput. Mater. Sci.* 68 (2013) 314–319.
- [22] R. Golesorkhtabar, P. Pavone, J. Spitaler, P. Puschnig, C. Draxl, *Comput. Phys. Comm.* 184 (2013) 1861–1873.
- [23] M.D. Segall, P.J.D. Lindan, M.J. Probert, C.J. Pickard, P.J. Hasnip, S.J. Clark, M.C. Payne, *J. Phys.: Condens. Matter.* 14 (2002) 2717.
- [24] G. Kresse, J. Furthmüller, *Phys. Rev. B* 54 (1996) 11169.
- [25] W.F. Perger, J. Criswell, B. Civalleri, R. Dovesi, *Comput. Phys. Comm.* 180 (2009) 1753–1759.
- [26] W. Voigt, *Lehrbuch Der Kristallphysik, Mit Ausschluss Der Kristalloptik*, Leipzig, Berlin, 1928.
- [27] R. Yu, J. Zhu, H.Q. Ye, *Comput. Phys. Comm.* 181 (2010) 671–675.
- [28] L. Vitos, *Computational Quantum Mechanics for Materials Engineers: The EMT0 Method and Applications*, Springer Science & Business Media, 2007.
- [29] A. Reuss, *Z. Angew. Math. Mech.* 9 (1929) 49–58.
- [30] Z. Hashin, S. Shtrikman, *J. Mech. Phys. Solids* 10 (1962) 343–352.
- [31] R. Hill, *Proc. Phys. Soc. A* 65 (1952) 349.
- [32] J.R. Rice, G.E. Beltz, Y. Sun, *Topics in Fracture and Fatigue*, Springer, New York, 1992, pp. 1–58.
- [33] G. Xu, A.S. Argon, M. Ortiz, *Phil. Mag. A* 75 (1997) 341–367.
- [34] A.V. Ponomareva, E.I. Isaev, Y.K. Vekilov, I.A. Abrikosov, *Phys. Rev. B* 85 (2012) 144117.
- [35] C. Zener, *Elasticity and Anelasticity of Metals*, University of Chicago press, 1948.
- [36] D.H. Chung, W.R. Buessem, *J. Appl. Phys.* 38 (1967) 2010–2012.
- [37] S.I. Ranganathan, M. Ostojia-Starzewski, *Phys. Rev. Lett.* 101 (2008) 055504.
- [38] G. Grimvall, B. Magyari-Köpe, V. Ozoliņš, K.A. Persson, *Rev. Modern Phys.* 84 (2012) 945.
- [39] M. Born, K. Huang, *Dynamical Theory of Crystal Lattices*, Clarendon press, 1954.
- [40] D.C. Wallace, *Thermodynamics of Crystals*, Wiley, New York, 1972.
- [41] J.H. Wang, J. Li, S. Yip, D. Wolf, S. Phillpot, *Physica A* 240 (1997) 396–403.
- [42] J. Zhou, R. Huang, *J. Mech. Phys. Solids* 56 (2008) 1609–1623.
- [43] Q. Wei, X.H. Peng, *Appl. Phys. Lett.* 104 (2014) 251915.
- [44] Z.H. Fu, Q.F. Zhang, D. Legut, C. Si, T.C. Germann, T. Lookman, S.Y. Du, J.S. Francisco, R.F. Zhang, *Phys. Rev. B* 94 (2016) 104103.
- [45] X.H. Zha, K. Luo, Q.W. Li, Q. Huang, J. He, X.D. Wen, S.Y. Du, *Europhys. Lett.* 111 (2015) 26007.
- [46] A. Meitzler, H.F. Tiersten, A.W. Warner, D. Berlincourt, G.A. Couquin, F.S. Welsh III, *IEEE Standard on Piezoelectricity*, Society, 1988.
- [47] <http://atzotgo.github.io/spglib/>.
- [48] A. van de Walle, G. Ceder, *J. Phase Equilib.* 23 (2002) 348.
- [49] H. Högborg, L. Hultman, J. Emmerlich, T. Joelsson, P. Eklund, J.M. Molina-Aldareguia, J.P. Palmquist, O. Wilhelmsson, U. Jansson, *Surf. Coat. Technol.* 193 (2005) 6–10.
- [50] G. Kresse, D. Joubert, *Phys. Rev. B* 59 (1999) 1758.
- [51] J.P. Perdew, K. Burke, M. Ernzerhof, *Phys. Rev. Lett.* 77 (1996) 3865.
- [52] D.M. Ceperley, B.J. Alder, *Phys. Rev. Lett.* 45 (1980) 566.
- [53] J.P. Perdew, A. Zunger, *Phys. Rev. B* 23 (1981) 5048.
- [54] M. Methfessel, A.T. Paxton, *Phys. Rev. B* 40 (1989) 3616.
- [55] H.J. Monkhorst, J.D. Pack, *Phys. Rev. B* 13 (1976) 5188.
- [56] X.D. Wei, B. Fragneaud, C.A. Marianetti, J.W. Kysar, *Phys. Rev. B* 80 (2009) 205407.
- [57] R.C. Cooper, C.G. Lee, C.A. Marianetti, X.D. Wei, J. Hone, J.W. Kysar, *Phys. Rev. B* 87 (2013) 035423.
- [58] Q. Peng, S. De, *Phys. Chem. Chem. Phys.* 15 (2013) 19427–19437.
- [59] Q. Peng, X.D. Wen, S. De, *RSC Adv.* 3 (2013) 13772–13781.
- [60] S. Wang, J.X. Li, Y.L. Du, C. Cui, *Comput. Mater. Sci.* 83 (2014) 290–293.
- [61] A.J. Mannix, X.F. Zhou, B. Kiraly, J.D. Wood, D. Alducin, B.D. Myers, X.L. Liu, B.L. Fisher, U. Santiago, J.R. Guest, *Science* 350 (2015) 1513–1516.
- [62] E. Cadelano, P.L. Palla, S. Giordano, L. Colombo, *Phys. Rev. B* 82 (2010) 235414.
- [63] A.G. Every, A.K. McCurdy, D.F. Nelson, *Second and Higher Order Elastic Constants*, Springer, Berlin, 1992.
- [64] C.h. Zha, H.w. Mao, R.J. Hemley, *Proc. Natl. Acad. Sci.* 97 (2000) 13494–13499.
- [65] J.Q. Wang, C.X. Zhao, C.Y. Niu, Q. Sun, Y. Jia, *J. Phys.: Condens. Matter* 2 (2016) 8.
- [66] B.B. Karki, L. Stixrude, S.J. Clark, M.C. Warren, G.J. Ackland, J. Crain, *Am. Miner.* 82 (1997) 51–60.
- [67] C.F. Cline, H.L. Dunegan, G.W. Henderson, *J. Appl. Phys.* 38 (1967) 1944–1948.
- [68] V. Milman, M.C. Warren, *J. Phys.: Condens. Matter* 13 (2001) 241.
- [69] Z.J. He, Z.H. Fu, D. Legut, X.H. Yu, Q.F. Zhang, V.I. Ivashchenko, S. Veprek, R.F. Zhang, *Phys. Rev. B* 93 (2016) 184104.
- [70] C. Wang, H.Y. Wang, T.L. Huang, X.N. Xue, F. Qiu, Q.C. Jiang, *Sci. Rep.* 5 (2015).
- [71] J.R. Gladden, J.H. So, J.D. Maynard, P.W. Saxe, Y. Le Page, *Appl. Phys. Lett.* 85 (2004) 392–394.
- [72] S.L. Shang, Y. Wang, Z.K. Liu, *Appl. Phys. Lett.* 90 (2007) 101909.
- [73] R.F. Zhang, Z.J. Lin, Y.S. Zhao, S. Veprek, *Phys. Rev. B* 83 (2011) 092101.
- [74] S. Lee, D.M. Bylander, L. Kleinman, *Phys. Rev. B* 45 (1992) 3245.
- [75] Y.P. Lu, D.W. He, *J. Appl. Phys.* 105 (2009) 083540.
- [76] W.J. Alton, A.J. Barlow, *J. Appl. Phys.* 38 (1967) 3817–3820.
- [77] A.H. Reshak, M. Jamal, *Int. J. Electrochem. Sci.* 8 (2013) 12252–12263.
- [78] O. Beckstein, J.E. Klepeis, G.L.W. Hart, O. Pankratov, *Phys. Rev. B* 63 (2001) 134112.
- [79] M. Iuga, G. Steinle-Neumann, J. Meinhardt, *Eur. Phys. J. B* 58 (2007) 127–133.
- [80] H. Niu, X.Q. Chen, S. Wang, D. Li, W.L. Mao, Y. Li, *Phys. Rev. Lett.* 108 (2012) 294–300.
- [81] D.G. Isaak, I. Ohno, *Phys. Chem. Miner.* 30 (2003) 430–439.
- [82] L. Sang, C.B. Vanpeteghem, S.V. Sinogeikin, J.D. Bass, *Am. Miner.* 96 (2011) 224–227.
- [83] M.J. Xing, B.H. Li, Z.T. Yu, Q. Chen, *RSC Adv.* 6 (2016) 32740–32745.